Investigation of a New Electrode Array Technology for a Central Auditory Prosthesis

Roger Calixto[1]*, Behrouz Salamat[1], Thilo Rode[1], Tanja Hartmann[1], Bart Volckaerts[2], Patrick Ruther[3], Thomas Lenarz[1], Hubert H. Lim[4]

1 Institute of Audioneurotechnology and Department of Experimental Otology, Hannover Medical University, Hannover, Germany, 2 Cochlear GmbH, Hannover, Germany, 3 Department of Microsystems Engineering (IMTEK) at the University of Freiburg, Freiburg, Germany, 4 Department of Biomedical Engineering, University of Minnesota, Minneapolis, Minnesota

Abstract

Ongoing clinical studies on patients recently implanted with the auditory midbrain implant (AMI) into the inferior colliculus (IC) for hearing restoration have shown that these patients do not achieve performance levels comparable to cochlear implant patients. The AMI consists of a single-shank array (20 electrodes) for stimulation along the tonotopic axis of the IC. Recent findings suggest that one major limitation in AMI performance is the inability to sufficiently activate neurons across the three-dimensional (3-D) IC. Unfortunately, there are no currently available 3-D array technologies that can be used for clinical applications. More recently, there has been a new initiative by the European Commission to fund and develop 3-D chronic electrode arrays for science and clinical applications through the NeuroProbes project that can overcome the bulkiness and limited 3-D configurations of currently available array technologies. As part of the NeuroProbes initiative, we investigated whether their new array technology could be potentially used for future AMI patients. Since the NeuroProbes technology had not yet been tested for electrical stimulation in an in vivo animal preparation, we performed experiments in ketamine-anesthetized guinea pigs in which we inserted and stimulated a NeuroProbes array within the IC and recorded the corresponding neural activation within the auditory cortex. We used 2-D arrays for this initial feasibility study since they were already available and were sufficient to access the IC and also demonstrate effective activation of the central auditory system. Based on these encouraging results and the ability to develop customized 3-D arrays with the NeuroProbes technology, we can further investigate different stimulation patterns across the ICC to improve AMI performance.

Introduction

Cochlear implants (CIs) are the most successful neuroprostheses to date with over 200,000 subjects implanted worldwide [1–3]. However, in cases where the cochlea or auditory nerve is congenitally malformed or damaged, a CI is not a viable option. In such cases the only commercially available alternative is the auditory brainstem implant [4,5], a device that stimulates the brainstem with surface electrodes. In general, these patients do not achieve hearing performance levels comparable to CI patients [6].

As an alternative, the auditory midbrain implant (AMI), which targets the central nucleus of the inferior colliculus (ICC) with a penetrating electrode array, was developed [7]. The AMI is in clinical trials and patients receive daily benefits from their implants [8,9]. However, as with brainstem implants, the AMI also does not achieve performance levels comparable to a CI. Based on recent human and animal studies [9–13], one major limitation is that the current single-shank AMI array (consisting of 20 linearly spaced electrodes) cannot sufficiently activate neurons across the three-

dimensional (3-D) IC structure for adequate spectral and temporal coding, which are important features for speech perception [14–16]. A single-shank array was implanted into the first AMI patients since no 3-D array technologies were available for clinical application [7] and this single-shank array technology had already been shown to be safe for implantation into the ICC [17,18].

More recently, the European Commission began the NeuroProbes (NP) project to fund and develop new 3-D, chronic array technologies to address the ongoing and significant need for such technologies for neuroscience investigations and clinical applications [19]. We assisted the NP project by testing their new silicon-based array technology in guinea pig experiments to assess whether the NP technology could be used for ICC stimulation and potentially in future AMI clinical trials.

The advantage of silicon-substrate electrode arrays compared to traditional microwires is that they can be fabricated with numerous sites in precise (with micron resolution) and closely spaced (tens of microns) configurations and integrated with electronics. There are other types of silicon-based array technol-

ogies currently available in the neural engineering field. The two major devices are known as the Utah array [20–22] and the NeuroNexus array (i.e., Michigan Probe [23–26]). Both have been successfully used for recording and stimulation applications in acute and chronic animals. The Utah array has also been used in humans for cortical recordings [27]. The major limitation with these devices is that they typically only span a two-dimensional (2-D) space. The Utah array consists of multiple shanks in a 3-D configuration with only one site at the tip of each shank, resulting in a 2-D pattern of sites. The lengths of the shanks can be altered to record or stimulate in different planes but they cannot fully span the 3-D space. The NeuroNexus array is a planar technology in which multiple shanks consisting of several sites along each shank can be configured in a 2-D pattern. There have been attempts at stacking these 2-D arrays into a 3-D configuration using special adapters (examples shown on NeuroNexus website: http://www. neuronexus.com) or superglue [28], but these solutions have resulted in a loss of precision and alignment between the stacked shanks and/or require a bulky interface, which is not favorable for chronic implementation [19].

The NP array takes advantage of the fabrication processes of both types of technologies described above. However, the key difference is that it uses a modular approach to create custom 3-D arrays. The NP array consists of a slim backbone or interface that allows individual shanks and/or groups of 2-D planar arrays to be precisely inserted into this backbone in a Lego©– like fashion [29,30]. This backbone is slim and connects to a highly flexible ribbon cable to reduce the bulkiness of the interface. It is also possible to incorporate fluidic channels through this interface connecting to some or all of the inserted shanks for drug delivery and chemical sensing, resulting in a fully integrated system [30,31]. Several prototype NP arrays have been developed and successfully inserted into cortical regions without breakage, have achieved recording of neural activity, and have maintained biocompatibility within brain tissue [32,33]. Further details on the fabrication process and various configurations of the NP arrays are provided in [29,30,32].

Considering the 3-D capabilities of the NP array and the need for 3-D stimulation within the ICC for improving the AMI, we tested the stimulation effects of the NP array in the ICC of the guinea pig. Since the NP technology had not yet been tested for stimulation in an in vivo preparation, our initial objective was to assess if we could electrically stimulate through the NP sites with sufficient current to activate the central auditory system. The shanks also required long lengths of 10 mm to reach the deep location of the ICC, and thus we assessed if the arrays were stiff and strong enough to be inserted through the tissue without breakage. We used 2-D arrays for this study since they were already available and would be sufficient to achieve our objectives, whereas a 3-D array customized to the ICC would require additional time and costs for development. Demonstrating the feasibility of stimulating deep brain structures with the NP arrays in this study will justify further development of 3-D NP arrays for the ICC that can lead to improved stimulation strategies for the AMI.

Methods

Anesthesia and surgery

Detailed methods have been presented previously [11,34]. Briefly, experiments were performed on three albino guinea pigs (494–630 g; DH; Harlan Laboratories, Horst, Netherlands) that were anesthetized with a ketamine (40 mg/kg) and xylazine (10 mg/kg) mixture with additional supplements to maintain an

areflexive state. Atropine sulfate (0.05 mg/kg) was administered subcutaneously to reduce bronchial secretions when necessary. Body temperature was maintained at $38\pm0.5°C$ with a water heated blanket, and heart rate and blood oxygen levels were monitored via pulse oximetry. The guinea pigs' care and all experiments were carried out in accordance with the German law for animal protection and were approved by the Landesamtes für Verbraucherschutz und Lebensmittelsicherheit (LAVES, registration number 05/1055).

The animal was placed in a stereotaxic frame (David Kopf Instruments, Tujunga, CA) with hollow ear bars to allow for calibrated closed-field acoustic stimulation. A craniotomy was performed exposing the right temporal and occipital lobes and the dura was then resected. The occipital lobe was carefully aspirated to provide visual access to the inferior colliculus. The NP array (Fig. 1; 4 shanks, 10 mm long, 8 IrOx sites/shank, 960 μm^2/site; impedances of 310–630 kΩ at 1 kHz) was then placed at a 45° angle to the sagittal plane and inserted into the inferior colliculus to be aligned along the tonotopic axis of the ICC [35,36]. Proper array placement in the ICC was confirmed by observing frequency response maps that exhibited an orderly shift from low to high frequencies for superficial to deeper locations, respectively, along a shank [35,37]. We implanted a 2-D NP array instead of a 3-D version in these initial experiments since 2-D arrays were already available that could achieve the objectives of our study in accessing and acutely stimulating the ICC. Future studies will assess the ability to implant and stimulate a 3-D NP array over longer periods.

For recording the cortical activity, a second array (8 shanks, 200 μm apart, 2 mm long, 4 Ir sites/shank, 413 μm^2/site; impedances of 1–2 MΩ at 1 kHz; NeuroNexus Technologies, Ann Arbor, MI, USA) was inserted into the primary auditory cortex (A1). The A1 area was identified by its clear tonotopic organization of low to high frequencies with a rostrolateral to caudomedial orientation within the auditory cortex [38,39]. The array was inserted approximately perpendicular to the cortical surface in an attempt to align each shank along a column in A1 [39,40]. The depth of the sites was controlled with current source density (CSD) analysis [41–43] so that one site per shank was positioned into the main input layer (III/IV) of A1. The one-dimensional CSD approximation provides a consistent represen-
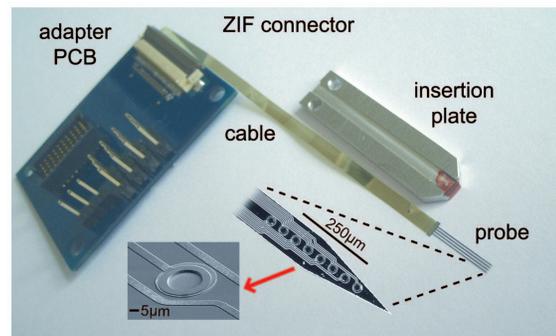
Figure 1. Comb-like, silicon-based NeuroProbes array with four 10-mm-long probe shafts separated by 400 μm. Each shank is comprised of eight IrOx electrode sites. The array is interconnected to a highly flexible polyimide ribbon cable interfacing with a zero insertion force (ZIF) connector on a printed circuit board (PCB) that was connected to the stimulator. For probe insertion, the probe comb is fixed adhesively to the insertion plate and attached to a micromanipulator. The 100-μm-thick probe shanks proved to be stiff enough for insertion into deep brain structures.
doi:10.1371/journal.pone.0082148.g001

tation for the current sinks and sources associated with columnar synaptic activity in the guinea pig auditory cortex [44,45]. Further details on how to perform the CSD analysis and to identify layer III/IV are provided in [46].

After array placements into ICC and A1, the brain surface was covered with agarose gel to minimize pulsations and drying. The A1 array was used to assess the activation properties of NP stimulation in online and offline analysis.

Stimulation and recording

Stimulation and recording were performed using a computer interfaced with TDT System 3 hardware (Tucker-Davis Technology, Alachua, FL) using custom written software with Matlab (Mathworks, Natick, MA). Acoustic stimulation was used to guide placement of arrays based on neural response patterns. In each animal, we then identified one stimulation site per shank on the NP array for a total of four sites that were in similar frequency regions of the ICC. We electrically stimulated each site with single biphasic pulses (cathodic-leading, 205 µs/phase) and recorded the corresponding neural activity on an A1 site in a similar frequency region. The following frequency regions were stimulated across animals: 15, 16, and 17 kHz. Stimulation level varied from 20–52 dB (in 2-dB steps relative to 1 µA; 10–398 µA). All stimuli were randomly presented for a total of 20 trials, including 20 spontaneous trials (i.e., no stimulus trials), at a rate of 2/s.

Analysis

We analyzed both A1 local field potentials (LFPs) and multi-unit activity (MUA) in response to ICC stimulation. The LFP responses recorded on our main input layer sites generally correspond to the synaptic input into layers III/IV of A1 whereas the MUA corresponds to the spiking pattern of multiple neurons surrounding the recording sites within layer III/IV [42,47]. LFP analysis was performed on the averaged unfiltered trials after removal of the stimulus artifact (Fig. 2A shows examples with artifact for better visualization of stimulus onset). Artifacts were removed by blanking the 1.5-ms period following stimulus onset for each trial and connecting the points before and after this window with a straight line. We then calculated the magnitude and area of the negative LFP peak as described elsewhere [11,48]. LFP threshold was defined as the level that elicited a response that was 3.5 times above the average background noise. We used this threshold method because it provided values that were consistent with those determined visually when selecting the level that elicited a noticeable LFP response above the background activity. MUA was displayed as post-stimulus time histograms with 1 ms bins (PSTHs; Fig. 2B) after artifact removal and filtering (300–3000 Hz) of each trial of data and detecting spikes that exceeded three times the standard deviation of the noise floor (Fig. 2B shows example of detected spikes). From the PSTHs, we calculated the driven spike rate (total spikes minus spontaneous spikes within a 30-ms window relative to stimulus onset) across different levels for further analysis. MUA threshold was defined as the lowest level that elicited a visible response above spontaneous activity for two consecutive PSTH level steps.

Results

We analyzed the LFP and MUA responses recorded in A1 due to ICC stimulation with the NP array. A total of 12 NP sites were stimulated across three animals with various current levels. In all three consecutive animals, we successfully inserted the NP array into the ICC without breakage and could deliver sufficient current
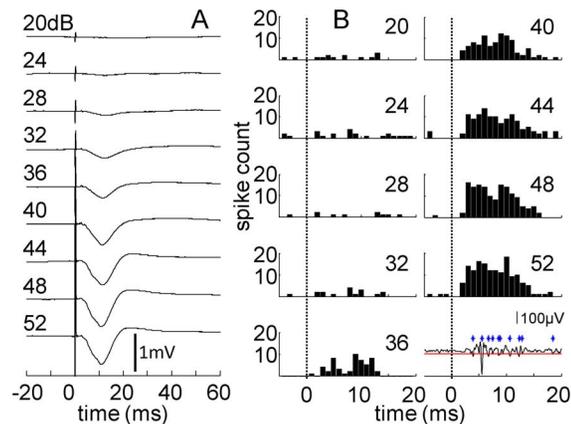

Figure 2. Raw data and PSTH plots. A) Averaged unfiltered raw data (20 sweeps) showing LFP in response to stimulation with an NP site from 20 to 52 dB relative to 1 µA (actual stimuli were 12–52 dB in 2-dB steps). The monotonic increase in LFP size with stimulation amplitude is evident. The LFP threshold is 28 dB in this example. B) PSTHs corresponding to the different stimulation levels indicated in each plot. PSTH bars represent 1 ms bins. The dotted line indicates stimulus onset at 0 ms. Bottom right trace is a single trial filtered for spikes with the artifact removed and showing multi-unit activity in response to a stimulation at 52 dB. Each detected spike is marked by an * with the red line indicating threshold for spike detection. The MUA threshold is 34 dB, which is higher than the LFP threshold.
doi:10.1371/journal.pone.0082148.g002

through the 12 sites to activate the central auditory system from the ICC up to A1.

LFP responses

Figure 2A presents A1 LFPs in response to stimulation for varying levels from threshold up to 52 dB (all values in dB relative to 1 µA). The LFP response consisted of a negative deflection that generally exhibited a monotonically increasing magnitude and area with higher current levels (Fig. 3A and 3B, respectively). The mean LFP threshold was 27.7 dB (SD: 5.5), which is approximately 24 µA. Encouragingly, the shape and monotonic nature of these LFP responses appear similar to what has been observed for ICC stimulation with the current AMI array [11,34]. Monotonic growth functions are important for auditory implants in enabling systematic control over loudness sensations with changes in current level. One main difference is that NP stimulation achieves lower LFP thresholds than what was previously observed for AMI stimulation (~63 µA; [49]) using similar stimulation and recording parameters (also in guinea pigs). These previous AMI thresholds were obtained by determining the highest level where the evoked potential could not be observed (i.e., a response that was lost in the spontaneous activity), which identifies a threshold level that is lower than what would be selected using our current method (i.e., the lowest amplitude with a detectable LFP). Yet, NP stimulation still achieved lower thresholds suggesting that this difference may be related to the significantly smaller sites of the NP array.

MUA responses

Figure 2B presents PSTHs for NP stimulation for the same data set used for the LFP responses in Fig. 2A. The MUA responses also generally exhibit monotonically increasing growth functions (Fig. 3C) consistent with the LFP responses. The mean MUA threshold was 33.5 dB (SD: 5.7), which is about 47 µA. Interestingly, these MUA thresholds were higher than what has been observed for AMI stimulation (~27 µA; [50]) using similar
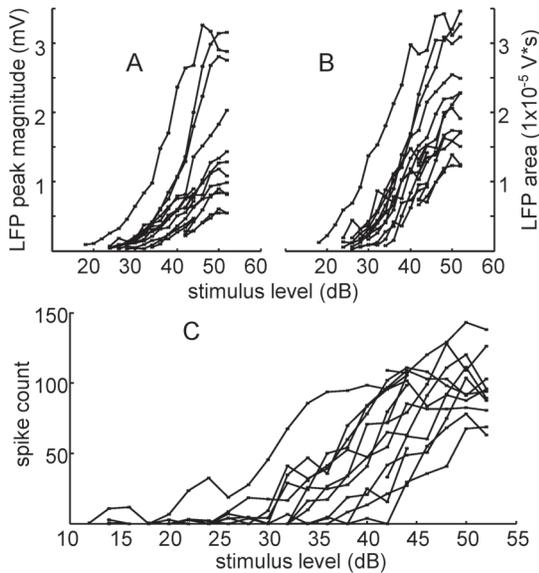
Figure 3. Rate growth curves recorded from A1 and pooled from all 12 stimulated NP sites. A) Growth rate of LFP peak magnitude versus stimulus level (in dB relative to 1 µA). B) Growth rate of LFP area versus stimulus level. C) Growth rate for multi-unit spikes versus stimulus level.
doi:10.1371/journal.pone.0082148.g003

stimulation and recording parameters and the same threshold method as in our study (also in guinea pigs). This result is in contrast to the lower LFP thresholds we observed for NP stimulation compared to AMI stimulation. It is possible that the smaller sites of the NP array will more effectively elicit LFP activity than spike activity (LFP thresholds were significantly lower than MUA thresholds; p<0.0001 using a two-tailed Welch's t-test), whereas the reverse is true for the AMI array. These discrepancies may also be due to the use of different breeds of guinea pigs or different array placements throughout the ICC or A1 across studies.

Discussion

We were able to successfully insert the NP array into the ICC without breakage. Considering the LFP and MUA thresholds and neural responses presented above, we have also shown that stimulation of the NP array can activate the central auditory system and exhibit similar growth function trends to those previously published for the current AMI array [49,50]. However, due to the significantly smaller sites of the NP array compared to the current AMI array (960 µm^2 versus 126,000 µm^2), one must consider the issue of safety limits for neural stimulation since it depends on the site area.

It is well known that total charge is the main factor eliciting neural activation with central stimulation [51]. Tissue damage to stimulation, on the other hand, is dependent on the synergy of the total injected charge per phase (i.e. sum of charge over time) and charge density per phase (i.e. total charge divided by surface area) [52,53]. A multi-study comparison has provided a "threshold" for tissue damage that can be modeled with a simple equation, known as the "Shannon curve", and a safety parameter k (lower k values correspond to more conservative stimulation regimes) that are described in [54]. A k value of 2 has been approximated as the border between safe and unsafe stimulation (for further details, see [53]). However, care should be taken when using this parameter.

This equation was largely based on stimulation studies performed with surface electrodes, and thus may overestimate the limits for safe stimulation with penetrating electrodes [55]. Furthermore, the k parameter was calculated based on a limited set of acute stimulation parameters and should be interpreted with care for other stimulation regimes.

Since activation levels (i.e., total charge) on the same order of magnitude were observed for both NP and AMI stimulation, the smaller electrode surface area for the NP sites will lead to higher charge density values, which in turn can lead to greater tissue damage at lower current levels [52,53]. Figure 4 shows the modeled charge per phase versus charge density per phase for both NP and AMI stimulation using the equation from [54]. Although only pulse widths of 200 µs/phase were delivered experimentally, we have included 100, 200, and 400 µs/phase for comparison. The limits of safe stimulation are approximated by the thick solid line (k = 2). The AMI can be safely stimulated up to about 62 dB (1259 µA) for 200 µs/phase pulses (charge = 0.25 µC and charge density = 199 µC/cm^2 on the plot). However, NP stimulation can only reach approximately 42 dB (charge = 0.025 µC and charge density = 2623 µC/cm^2) before exceeding the safety limit. Thus, it is apparent that the total charge range for NP stimulation from threshold to this safety limit (i.e., dynamic range) is smaller than for AMI stimulation.

It is not yet clear if stimulation of smaller and possibly different neural clusters with the NP sites will elicit similar or different auditory percepts as those achieved with AMI sites. This needs to be further investigated in behavioral animal models. However, the key advantage of the NP technology is that a greater number of sites can potentially be implanted throughout the 3-D ICC. It is possible that simultaneous stimulation of multiple sites may enable louder percepts with lower current levels, thus remaining within the safety limits for stimulation. In fact, the ICC normally codes for different sound features through activation of multiple neurons throughout its 3-D structure [56–58]. Therefore, a 3-D NP array may provide more realistic activation patterns throughout the ICC to improve overall hearing performance. In this initial feasibility study, we have shown that a 2-D NP array can access and activate
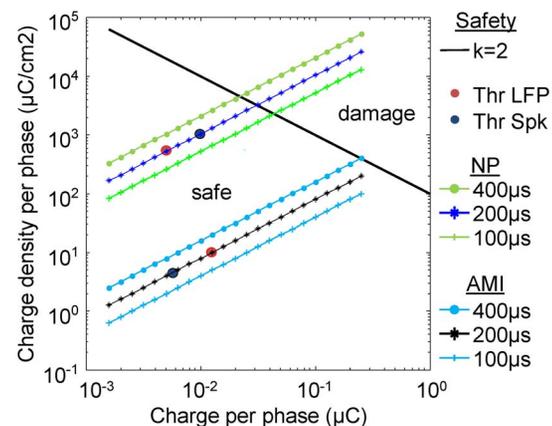

Figure 4. Modeled safe stimulation parameters. Stimulation above the solid black line (k = 2) has been shown to induce tissue damage and co-varies with total charge and charge density per pulse phase. The curves with different symbols reflect how charge density changes with increasing charge per phase for either the NP or AMI sites, i.e., for different site areas, for three different pulse widths each. The local field potential (LFP, red dot, 200 µs/phase) and spike (Spk, blue dot, 200 µs/phase) thresholds obtained from animal studies are labeled on the plot for direct comparison.
doi:10.1371/journal.pone.0082148.g004

central auditory pathways. The next stage of research will be to develop appropriate 3-D arrays that can more fully activate the ICC over longer periods and eventually translate this NP technology into future AMI patients.

Acknowledgments

Author Contributions

Conceived and designed the experiments: RC BV PR TL HHL. Performed the experiments: RC BS TH TR. Analyzed the data: RC. Contributed reagents/materials/analysis tools: BV PR. Wrote the paper: RC HHL. Designed electrode: PR. Initiated collaboration and proposed experiment set: BV.

References

1. Wilson BS, Dorman MF (2008) Cochlear implants: a remarkable past and a brilliant future. Hear Res 242: 3–21.

2. Zeng FG, Rebscher S, Harrison W, Sun X, Feng H (2008) Cochlear implants: system design, integration, and evaluation. IEEE Rev Biomed Eng 1: 115–142.

3. Rauschecker JP, Shannon RV (2002) Sending sound to the brain. Science 295: 1025–1029.

4. Colletti V, Shannon RV, Carner M, Veronese S, Colletti L (2009) Progress in restoration of hearing with the auditory brainstem implant. Progress in brain research 175: 333–345.

5. Schwartz MS, Otto SR, Shannon RV, Hitselberger WE, Brackmann DE (2008) Auditory brainstem implants. Neurotherapeutics 5: 128–136.

6. Colletti V, Shannon R, Carner M, Veronese S, Colletti L (2009) Outcomes in Nontumor Adults Fitted With the Auditory Brainstem Implant: 10 Years' Experience. Otol Neurotol 30: 614–618.

7. Lenarz T, Lim HH, Reuter G, Patrick JF, Lenarz M (2006) The auditory midbrain implant: a new auditory prosthesis for neural deafness-concept and device description. Otol Neurotol 27: 838–843.

8. Lim HH, Lenarz T, Joseph G, Battmer RD, Samii A, et al. (2007) Electrical stimulation of the midbrain for hearing restoration: insight into the functional organization of the human central auditory system. J Neurosci 27: 13541–13551.

9. Lim HH, Lenarz M, Lenarz T (2009) Auditory midbrain implant: a review. Trends Amplif 13: 149–180.

10. Lim HH, Lenarz T, Joseph G, Battmer RD, Patrick JF, et al. (2008) Effects of phase duration and pulse rate on loudness and pitch percepts in the first auditory midbrain implant patients: Comparison to cochlear implant and auditory brainstem implant results. Neuroscience 154: 370–380.

11. Calixto R, Lenarz M, Neuheiser A, Scheper V, Lenarz T, et al. (2012) Co-activation of different neurons within an isofrequency lamina of the inferior colliculus elicits enhanced auditory cortical activation J Neurophysiol published ahead of print May 23, 2012 doi:10.1152/jn.00111.02012

12. McKay CM, Lim HH, Lenarz T (2013) Temporal processing in the auditory system : insights from cochlear and auditory midbrain implantee. J Assoc Res Otolaryngol 14: 103–124.

13. Lim HH, Lenarz M, Joseph G, Lenarz T (2013) Frequency representation within the human brain: Stability versus plasticity. Sci Rep 3: 1474.

14. Shannon RV, Zeng FG, Kamath V, Wygonski J, Ekelid M (1995) Speech recognition with primarily temporal cues. Science 270: 303–304.

15. Nie K, Barco A, Zeng FG (2006) Spectral and temporal cues in cochlear implant speech perception. Ear Hear 27: 208–217.

16. Friesen LM, Shannon RV, Baskent D, Wang X (2001) Speech recognition in noise as a function of the number of spectral channels: comparison of acoustic hearing and cochlear implants. J Acoust Soc Am 110: 1150–1163.

17. Samii A, Lenarz M, Majdani O, Lim HH, Samii M, et al. (2007) Auditory midbrain implant: a combined approach for vestibular schwannoma surgery and device implantation. Otol Neurotol 28: 31–38.

18. Lenarz M, Lim HH, Lenarz T, Reich U, Marquardt N, et al. (2007) Auditory midbrain implant: histomorphologic effects of long-term implantation and electric stimulation of a new deep brain stimulation array. Otol Neurotol 28: 1045–1052.

19. Neves HP, Ruther P (2007) The NeuroProbes Project. Conf Proc IEEE Eng Med Biol Soc 2007: 6443–6445.

20. Campbell PK, Jones KE, Huber RJ, Horch KW, Normann RA (1991) A silicon-based, three-dimensional neural interface: manufacturing processes for an intracortical electrode array. IEEE Trans Biomed Eng 38: 758–768.

21. Rousche PJ, Normann RA (1998) Chronic recording capability of the Utah Intracortical Electrode Array in cat sensory cortex. J Neurosci Methods 82: 1–15.

22. Rousche PJ, Normann RA (1999) Chronic intracortical microstimulation (ICMS) of cat sensory cortex using the Utah Intracortical Electrode Array. IEEE Trans Rehabil Eng 7: 56–68.

23. Anderson DJ, Najafi K, Tanghe SJ, Evans DA, Levy KL, et al. (1989) Batch-fabricated thin-film electrodes for stimulation of the central auditory system. IEEE Trans Biomed Eng 36: 693–704.

24. Najafi K, Wise KD, Mochizuki T (1985) A high-yield IC-compatible multichannel recording array. IEEE Trans Electron Dev 32: 1206–1211.

25. Vetter RJ, Williams JC, Hetke JF, Nunamaker EA, Kipke DR (2004) Chronic neural recording using silicon-substrate microelectrode arrays implanted in cerebral cortex. IEEE Trans Biomed Eng 51: 896–904.

26. Weiland JD, Anderson DJ (2000) Chronic neural stimulation with thin-film, iridium oxide electrodes. IEEE Trans Biomed Eng 47: 911–918.

27. Hochberg LR, Bacher D, Jarosiewicz B, Masse NY, Simeral JD, et al. (2012) Reach and grasp by people with tetraplegia using a neurally controlled robotic arm. Nature 485: 372–375.

28. Ogawa T, Riera J, Goto T, Sumiyoshi A, Nonaka H, et al. (2011) Large-scale heterogeneous representation of sound attributes in rat primary auditory cortex: from unit activity to population dynamics. J Neurosci 31: 14639–14653.

29. Aarts AA, Neves HP, Ulbert I, Wittner L, Grand L, et al. (2008) A 3D slim-base probe array for in vivo recorded neuron activity. Conf Proc IEEE Eng Med Biol Soc 2008: 5798–5801.

30. Neves HP, Orban GA, Koudelka-Hep M, Stieglitz T, Ruther P (2007) Development of modular multifunctional probe arrays for cerebral applications. Conf Proc IEEE EMBS Neural Eng 3: 104–109.

31. Frey O, van der Wal PD, Spieth S, Brett O, Seidl K, et al. (2011) Biosensor microprobes with integrated microfluidic channels for bi-directional neuro-chemical interaction. J Neural Eng 8: 066001.

32. Kisban S, Janssen M, Herwik S, Stieglitz T, Paul O, et al. (2008) Hybrid microprobes for chronic implantation in the cerebral cortex. Conf Proc IEEE Eng Med Biol Soc 2008: 2016–2019.

33. Grand L, Wittner L, Herwik S, Gothelid E, Ruther P, et al. (2010) Short and long term biocompatibility of NeuroProbes silicon probes. J Neurosci Methods 189: 216–229.

34. Neuheiser A, Lenarz M, Reuter G, Calixto R, Nolte I, et al. (2010) Effects of pulse phase duration and location of stimulation within the inferior colliculus on auditory cortical evoked potentials in a guinea pig model. J Assoc Res Otolaryngol 11: 689–708.

35. Snyder RL, Bierer JA, Middlebrooks JC (2004) Topographic spread of inferior colliculus activation in response to acoustic and intracochlear electric stimulation. J Assoc Res Otolaryngol 5: 305–322.

36. Malmierca MS, Rees A, Le Beau FE, Bjaalie JG (1995) Laminar organization of frequency-defined local axons within and between the inferior colliculi of the guinea pig. J Comp Neurol 357: 124–144.

37. Lim HH, Anderson DJ (2006) Auditory cortical responses to electrical stimulation of the inferior colliculus: implications for an auditory midbrain implant. J Neurophysiol 96: 975–988.

38. Redies H, Sieben U, Creutzfeldt OD (1989) Functional subdivisions in the auditory cortex of the guinea pig. J Comp Neurol 282: 473–488.

39. Wallace MN, Rutkowski RG, Palmer AR (2000) Identification and localisation of auditory areas in guinea pig cortex. Exp Brain Res 132: 445–456.

40. Abeles M, Goldstein MH, Jr. (1970) Functional architecture in cat primary auditory cortex: columnar organization and organization according to depth. J Neurophysiol 33: 172–187.

41. Muller-Preuss P, Mitzdorf U (1984) Functional anatomy of the inferior colliculus and the auditory cortex: current source density analyses of click-evoked potentials. Hear Res 16: 133–142.

42. Mitzdorf U (1985) Current source-density method and application in cat cerebral cortex: investigation of evoked potentials and EEG phenomena. Physiol Rev 65: 37–100.

43. Kral A, Hartmann R, Tillein J, Heid S, Klinke R (2000) Congenital auditory deprivation reduces synaptic activity within the auditory cortex in a layer-specific manner. Cereb Cortex 10: 714–726.

44. Lim HH, Anderson DJ (2007) Antidromic activation reveals tonotopically organized projections from primary auditory cortex to the central nucleus of the inferior colliculus in guinea pig. J Neurophysiol 97: 1413–1427.

45. Middlebrooks JC (2008) Auditory cortex phase locking to amplitude-modulated cochlear implant pulse trains. J Neurophysiol 100: 76–91.

46. Calixto R, Lenarz M, Neuheiser A, Scheper V, Lenarz T, et al. (2012) Coactivation of different neurons within an isofrequency lamina of the inferior colliculus elicits enhanced auditory cortical activation. J Neurophysiol 108: 1199–1210.

47. Eggermont JJ, Smith GM (1995) Synchrony between single-unit activity and local field potentials in relation to periodicity coding in primary auditory cortex. J Neurophysiol 73: 227–245.

48. Calixto R, Lenarz M, Neuheiser A, Scheper V, Lenarz T, et al. (2012) Co-activation of different neurons within an isofrequency lamina of the inferior colliculus elicits enhanced auditory cortical activation. J Neurophysiol.

49. Neuheiser A, Lenarz M, Reuter G, Calixto R, Nolte I, et al. (2010) Effects of Pulse Phase Duration and Location of Stimulation Within the Inferior Colliculus on Auditory Cortical Evoked Potentials in a Guinea Pig Model. Journal of the Association for Research in Otolaryngology : JARO.

50. Lenarz M, Lim HH, Patrick JF, Anderson DJ, Lenarz T (2006) Electrophysiological validation of a human prototype auditory midbrain implant in a guinea pig model. J Assoc Res Otolaryngol 7: 383–398.

51. Rattay F (1987) Ways to approximate current-distance relations for electrically stimulated fibers. J Theor Biol 125: 339–349.

52. McCreery DB, Agnew WF, Yuen TG, Bullara L (1990) Charge density and charge per phase as cofactors in neural injury induced by electrical stimulation. IEEE Trans Biomed Eng 37: 996–1001.

53. Merrill DR, Bikson M, Jefferys JG (2005) Electrical stimulation of excitable tissue: design of efficacious and safe protocols. J Neurosci Methods 141: 171–198.

54. Shannon RV (1992) A model of safe levels for electrical stimulation. IEEE Trans Biomed Eng 39: 424–426.

55. McCreery D, Pikov V, Troyk PR (2010) Neuronal loss due to prolonged controlled-current stimulation with chronically implanted microelectrodes in the cat cerebral cortex. J Neural Eng 7: 036005.

56. Ehret G (1997) The auditory midbrain, a "shunting yard" of acoustical information processing. In: Ehret G, Romand R, editors. The Central Auditory System. New York: Oxford University Press, Inc. pp. 259–316.

57. Rees A, Langner G (2005) Temporal coding in the auditory midbrain. In: Winer JA, Schreiner CE, editors. The Inferior Colliculus. New York: Springer Science+Business Media, Inc. pp. 346–376.

58. Oliver DL (2005) Neuronal organization in the inferior colliculus. In: Winer JA, Schreiner CE, editors. The Inferior Colliculus. New York: Springer Science+Business Media, Inc. pp. 69–114.